

## Research Article

# Crystalline Characteristic Effect of In Situ Interaction between ZnO and Pht on Inducing $\beta$ Nucleation of Isotactic Polypropylene

Shuya Cheng,<sup>1</sup> Kai Zhang ,<sup>1,2</sup> Guomin Xu,<sup>1,2</sup> Chunyan Shan,<sup>2</sup> Min He,<sup>1</sup> Shuhao Qin,<sup>1,2</sup> and Jie Yu<sup>1,2</sup>

<sup>1</sup>College of Materials Science and Metallurgy, Guizhou University, Guiyang 550025, China

<sup>2</sup>National Engineering Research Center for Compounding and Modification of Polymeric Materials, Guiyang 550014, China

Correspondence should be addressed to Kai Zhang; k.zhang2008@qq.com

Received 22 December 2021; Revised 28 March 2022; Accepted 27 April 2022; Published 27 May 2022

Academic Editor: Wenbing Hu

Copyright © 2022 Shuya Cheng et al. This is an open access article distributed under the Creative Commons Attribution License, which permits unrestricted use, distribution, and reproduction in any medium, provided the original work is properly cited.

The  $\beta$ -nucleating agent ( $\beta$ -NA), zinc phthalate (ZnPht), was prepared from a mixture of zinc oxide (ZnO) and phthalic anhydride (Pht) during the extrusion of isotactic polypropylene (iPP). To establish the relationship between the crystalline characteristic of ZnO and the crystallization of iPP, single-crystalline ZnO (ZnO(S)) and polycrystalline ZnO (ZnO(P)) were selected and mixed with Pht, respectively, to in situ inducing the  $\beta$ -crystal form of iPP ( $\beta$ -iPP). Compared to ZnO(S)/Pht, ZnO(P)/Pht has the selectivity of  $\beta$ -crystal nucleation during the crystallization of iPP; indeed, the relative content of  $\beta$ -crystal ( $k_{\beta}$ ) improved from 18.0% for ZnO(S)/Pht/iPP to 84.6% for ZnO(P)/Pht/iPP. Moreover, the impact strength of the ZnO(P)/Pht/iPP was nearly 2.0 times greater than pure iPP; for ZnO(S)/Pht/iPP, it was approximately 1.4 times greater than pure iPP. To explain these phenomena, we propose a mechanism that the content of ZnPht generated by ZnO(P)/Pht is more than that of ZnO(S)/Pht during its in situ reaction; evidence from Fourier transform infrared spectroscopy, wide-angle X-ray diffraction, and thermogravimetric infrared spectroscopy analysis was consistent with this mechanism. This study may provide a new perspective to control the crystal type of polymorphic polymer by adjusting the crystalline characteristic of the nucleating agent.

## 1. Introduction

Isotactic polypropylene (iPP) is widely used in automotive, construction, packaging, and other fields owing to its excellent physical properties and exceptional chemical resistance. As a typical semicrystalline polymer, iPP is well known for its four crystal forms ( $\alpha$ ,  $\beta$ ,  $\gamma$ , and smectic) [1–3]. Among the four crystal forms, the  $\beta$ -crystal form of iPP ( $\beta$ -iPP) has drawn great attention in industrial applications for its outstanding toughness and high impact resistance [4–7]. The  $\beta$ -crystal is a metastable crystalline phase that can only be available under certain situations [8–11]. Among them, adding the  $\beta$ -nucleating agent ( $\beta$ -NA) is considered the most convenient and effective way to obtain high content of  $\beta$ -iPP.

Nowadays, organic carboxylate metal salts (e.g., calcium pimelate and zinc adipate) [12–15], rare Earth compounds [16] (e.g.,  $\text{WBG}$ ,  $\text{Ca}_x\text{La}_{1-x}(\text{LIG1})_m(\text{LIG2})_n$ , where  $x$  and  $1-x$  represent the ratio of  $\text{Ca}^{2+}$  and  $\text{La}^{3+}$ , LIG1 and LIG2 denote

dicarboxylic acid and amide-type ligand, and  $m$  and  $n$  indicate coordination number, respectively), and aromatic amide compounds [17–19] (e.g., DCHT and DCHN refer to  $\text{N,N}'$ -dicyclohexylterephthalamide and  $\text{N,N}'$ -dicyclohexyl-2,6-naphthalenedicarboxamide, respectively) are used as  $\beta$ -NAs. Among these  $\beta$ -NAs, organic carboxylate metal salts display great superiority because of their relatively high nucleation efficiencies and good compatibility with iPP. The  $\beta$ -crystal nucleation of iPP employed by organic carboxylate metal salts has been studied by many researchers for years.

Shi et al. [20] discovered for the first time that a two-component complex of certain dibasic acids and certain metal compounds of group IIA in the periodic table can induce the formation of  $\beta$ -crystal in iPP. Their discovery opened a new chapter in the research of this type of  $\beta$ -NAs. Subsequently, the zinc, magnesium, calcium, and barium salts of malonic acid are confirmed as  $\beta$ -NAs for iPP by Dou et al. [21]. Moreover, a series of ortho dicarboxylates,

especially the bicycle [2.2.1] hept-5-ene-2,3-dicarboxylic acid salts, have been studied by Zhao et al. [12]. Recently, Zhao et al. [1] demonstrated that zinc phthalate (ZnPht) is a highly efficient  $\beta$ -NA and directly added zinc oxide (ZnO) and phthalic anhydride (Pht), the reaction precursors of ZnPht, into the extrusion process of iPP, which achieved the higher  $\beta$ -crystal nucleation efficiency. Due to the biocompatibility, chemical stability, and high photosensitivity of ZnO, the compatibility of Pht and iPP, and the high disperse of in situ synthesis,  $\beta$ -iPP was induced by ZnO and Pht by in situ synthesis has drawn wide attention. However, few people focused on the effect of crystalline characteristics of ZnO and Pht on  $\beta$ -iPP crystallization. The relationship between  $\beta$ -iPP crystallization and crystalline characteristic of ZnO and Pht is far from being fully understood. The study of the effect of crystalline characteristics of ZnO and Pht on  $\beta$ -iPP crystallization is beneficial to the application of ZnO and Pht as  $\beta$ -NA, meanwhile laying a foundation for understanding the mechanism of the generation of the  $\beta$ -iPP. Due to the low melting point of Pht, it is molten in the process of iPP processing. Therefore, the influence of ZnO with different crystalline characteristics in the presence of Pht on  $\beta$ -iPP crystallization was studied.

In this work, we choose two kinds of crystals, one is single-crystalline ZnO, and the other is polycrystalline ZnO (single-crystalline ZnO is abbreviated as ZnO(S), and polycrystalline ZnO is abbreviated as ZnO(P)) to induce  $\beta$ -iPP in situ with the presence of Pht. Here, both the crystalline shapes and structures of ZnO(S) and ZnO(P) have been characterized at first. Besides, the nucleation efficiencies, mechanical behavior, and isothermal crystallization behavior of nucleated iPP were conducted. Furthermore, the mechanism of crystalline characteristics of ZnO on the discrepancy of iPP crystal was studied and proved. This work provides a new perspective to control the crystal type of polymer by adjusting the crystalline characteristic of the nucleating agent.

## 2. Experimental

**2.1. Materials.** The isotactic polypropylene (iPP) (trade name: T30S;  $M_w$ :  $2.7 \times 10^5$  g/mol; PDI: 3.0) was supplied by Lanzhou Petrochemical Company (China), with a melt flow index (MFI) of 3.0 g/10 min ( $230^\circ\text{C}/2.16$  kg). Analytical reagent-grade o-Phthalic anhydride (Pht) and zinc oxide (ZnO) were purchased from Shanghai Macklin Biochemical Co., Ltd.

**2.2. Samples Preparation.** Firstly, ZnO(S) and ZnO(P) were mixed with Pht in a molar ratio of 1:1, respectively. Then, mixed powders of 0.2 wt% (relative to the pure iPP) were blended uniformly with iPP granules and extruded by a twin-screw extruder (CET-20, Nanjing Coperion Keya Machinery Co., Ltd., China). The extruder temperature is set at 190, 195, 200, 200, 195, and  $190^\circ\text{C}$  from the feed zone to the die. Finally, the composite granules were injected into standard specimens with the help of an injection-molding machine (130SE, Donghua Machinery Co., Ltd., China). The injection-

molding machine temperature was set at 210, 205, and  $200^\circ\text{C}$  in the compression zone, metering zone, and nozzle zone, respectively. The samples were named ZnO(S)/Pht/iPP and ZnO(P)/Pht/iPP, respectively. Meanwhile, a pure iPP sample was prepared in the same way for comparison.

### 2.3. Characterizations

**2.3.1. Mechanical Property.** Dumbbell-shaped samples were tested according to standard GB/T 1040-2018 using Microcomputer controlled electronic universal testing machine (CMT6104, MTS Systems, Shanghai, China) for tensile testing, and samples were elongated at a speed of 50 mm/min. Rectangular samples with a 2 mm “V” notch were tested on an impact tester (ZBC1400-B, MTS Systems, Shanghai, China) for impact strength tests. Every mechanical property experiment reported is the average of five independent measurements.

**2.3.2. Differential Scanning Calorimetry.** The crystallization peak temperature, the  $\beta$ -crystal content, and isothermal crystallization kinetics were investigated using differential scanning calorimetry (DSC, Q10, TA). The relative content of  $\beta$ -crystal from DSC ( $k_{\beta(\text{DSC})}$ ) was calculated by the following equation:

$$k_{\beta(\text{DSC})} = \frac{X_{\beta}}{X_{\beta} + X_{\alpha}}, \quad (1)$$

where  $X_{\alpha}$  and  $X_{\beta}$  were calculated by

$$X_i = \frac{\Delta H_i}{\Delta H_i^{\theta}}, \quad (2)$$

where  $X_i$  represents the crystallinity of  $\alpha$ -crystal form or  $\beta$ -crystal form,  $\Delta H_i$  represents the melting enthalpy of  $\alpha$ -crystal form or  $\beta$ -crystal form obtained from DSC curve, and  $\Delta H_i^{\theta}$  represents the standard melting enthalpy of perfect crystal in  $\alpha$ -crystal form or  $\beta$ -crystal form, where  $\Delta H_{\alpha}^{\theta}$  is 177 J/g and  $\Delta H_{\beta}^{\theta}$  is 168.5 J/g [22].

All weighed samples (5–10 mg) were placed in a dry nitrogen atmosphere with a flow of 50 ml/min. Firstly, samples have been rapidly heated from room temperature to  $200^\circ\text{C}$  and maintained for 5 min to release the thermal history. Subsequently, samples were cooled to  $50^\circ\text{C}$  at a rate of  $10^\circ\text{C}/\text{min}$  and then heated to  $200^\circ\text{C}$  at the same rate. For the isothermal crystallization kinetics study, the samples were cooled to the isothermal crystallization temperature ( $T_C$ ) at the maximum achievable rate of DSC and held for a period of time until the isothermal crystallization was complete. The  $T_C$  values of this work range from 128 to  $132^\circ\text{C}$ .

**2.3.3. Wide-Angle X-Ray Diffraction.** The phase composition was characterized by wide-angle X-ray diffraction (WAXD, Bruker D8 Advance) equipped with a Cu K $\alpha$  radiation ( $\lambda = 1.54 \text{ \AA}$ ,  $V = 40.0$  kv, and  $I = 40.0$  mA) at a scan rate of  $5^\circ/\text{min}$  for diffraction angles ( $2\theta$ ) ranging from 5 to  $90^\circ$ .

**2.3.4. Polarized Optical Microscopy Test.** The crystal morphologies and crystal growing process of samples were investigated using Polarized optical microscopy (POM; Sunny XP-P). The samples were pressed into films between microscopy coverslips and slides above the melting point and heated to 200°C for 5 min, cooled, and held at 130°C to complete the crystallization.

**2.3.5. Fourier Transform Infrared Spectroscopy.** Fourier transform infrared (FTIR) spectra of the samples were performed using a Nicolet 6700 FTIR spectrometer (Thermo Fisher, USA) and the classical KBr disk method at a range of 400–4000  $\text{cm}^{-1}$  at a resolution of 4  $\text{cm}^{-1}$ , and 32 scans were recorded for signal-averaging.

**2.3.6. X-Ray Photoelectron Spectroscopy.** X-ray-photoelectron spectroscopy (XPS) measurements were operated by K-Alpha at 12 kv voltage with Al  $K\alpha$  as the X-ray source.

**2.3.7. BET Surface Areas.** BET surface areas were recorded by Quantachrome NOVA 1000 e at 77 K after the products were degassed at 350°C for 3 h in a vacuum.

**2.3.8. Thermogravimetric Infrared Spectroscopy.** Thermal behaviors of ZnO and Pht were measured using thermogravimetric infrared spectroscopy (TG-FTIR; TG209F1 Libra/Nicolet 6700) under a dry nitrogen atmosphere at a heating rate of 10°C/min from 32°C to 800°C.

**2.3.9. Transmission Electron Microscopy.** The morphology of ZnO was observed by transmission electron microscopy (TEM, JEOL JEM 2100F) and high-resolution TEM (HRTEM), and selected area electron diffraction (SAED) was implemented in conjunction with the TEM measurements.

### 3. Results and Discussion

**3.1. The Crystalline Characteristic of ZnO(S) and ZnO(P).** The crystalline characteristics of ZnO(S) and ZnO(P) are shown in Figure 1. According to Figures 1(a)–1(b), ZnO(S) has a columnar shape and the crystalline size is between 80 nm and 380 nm. The HRTEM image shows lattice fringes of 0.162 nm, which should be referred to as the wurtzite ZnO (110) crystal planes. Figure 1(d) is the SAED pattern of ZnO(S), which exhibits a regularly arranged diffraction spot, indicating a single crystalline structure, and the two spots from the center outward have radii of 0.247 and 0.109 nm, corresponding to the (101) and (203) crystal planes of ZnO, respectively. In Figures 1(e)–1(f), the aggregates of ZnO(P) display flakes, and particle size is between 60 nm and 370 nm, almost equal to ZnO(S). However, the size of the single-crystalline grain is much smaller than 100 nm. As shown in Figure 1(g), the lattice spacing of ZnO(P) measured from the HRTEM image is 0.24 nm, corresponding to the (101) crystal plane. In the SAED image of ZnO(P) shown in Figure 1(h), multiple spots are seen on the circumference, indicative of different existing orientations, and the six

circulars from the center outward have radii of 0.247, 0.191, 0.147, 0.130, 0.123, and 0.109 nm, corresponding to the (101), (102), (103), (004), (202), and (203) crystal planes of ZnO, respectively. The WAXD patterns of ZnO(S) and ZnO(P) are shown in Figure 1(i), and ZnO(S) and ZnO(P) can be seen with different facet exposures, which can be clearly indexed to the wurtzite ZnO crystal structure (JCPDS Card No. 36-1451). XPS analyses are used to investigate the surface structure of ZnO(S) and ZnO(P). As shown in Figure 1(j), Zn 2p XPS spectra of ZnO(S) and ZnO(P) are analogous in their location and distribution. The O 1s spectra can be divided into two bands, shown in Figure 1(k) and Figure 1(l). According to these studies [23–25], the bands at about 530 eV are related to the ZnO crystal lattice oxygen ( $O_L$ ), and bands at about 531 eV are due to surface chemisorbed oxygen ( $O_C$ ) or OH. As displayed in Table 1, the relative percentages of the  $O_C$  or OH are 47.8% and 53.1% for ZnO(S) and ZnO(P), respectively. This demonstrated that the ZnO(P) may attract more oxygen species or OH. According to the literature [26], surface hydroxyl is an important reaction active species. Therefore, the reaction activity of samples would increase as the relative percentage of the  $O_C$  or OH component increased. Furthermore, BET surface area is one of the essential influence factors on reactivity. In general, reactivity increased as the BET surface area increased. From Table 1, it is noted that the discrepancy of BET surface area for ZnO(S) and ZnO(P) is very large. The BET surface area of ZnO(P) is 44.3  $\text{m}^2\cdot\text{g}^{-1}$ , which is 19 times bigger than the BET surface area of ZnO(S) of 2.3  $\text{m}^2\cdot\text{g}^{-1}$ , so the reactivity of ZnO(P) is higher than ZnO(S).

**3.2. The Nucleation of ZnO(S)/Pht and ZnO(P)/Pht in iPP.** The difference in crystalline characteristics of ZnO(S) and ZnO(P) with the presence of Pht may lead to the difference in nucleation in iPP. DSC is an effective method for characterizing the crystallization and melting behaviors of samples. In Figure 2(a), all samples provided one exothermic peak but the peak crystallization temperature ( $T_p$ ) was different. The values of  $T_p$  slightly increased, from 116.1 for pure iPP to 122.4 and 123.8°C for ZnO(S)/Pht/iPP and ZnO(P)/Pht/iPP, respectively. On the one hand, the evident change in these  $T_p$  indicates that  $\beta$ -NA influences the nonisothermal crystallization behavior of samples. On the other hand, higher  $T_p$  is suggestive of a dramatic decrease in supercooling ( $\Delta T = T_m^\theta - T_p$ , where  $T_m^\theta$  represents the equilibrium melting temperature, and  $T_p$  represents the crystallization temperature) needed to initiate the crystallization process, providing a greater tendency for crystallization and, thus, the faster speed for crystallization. These results confirm the effective nucleating of both ZnO(S)/Pht and ZnO(P)/Pht, and the nucleation efficiency of ZnO(P)/Pht is higher than that of ZnO(S)/Pht. In Figure 2(b), pure iPP provided only one endothermic peak at about 163°C, ascribed to the melting peak of  $\alpha$ -crystal. For ZnO(S)/Pht/iPP and ZnO(P)/Pht/iPP, besides the melting peak of  $\alpha$ -crystal, the melting peak of  $\beta$ -crystal also appears at about 151°C. It is worth noting that the melting peak of  $\alpha$ -crystal of ZnO(P)/Pht/iPP is divided into two temperatures: the lower

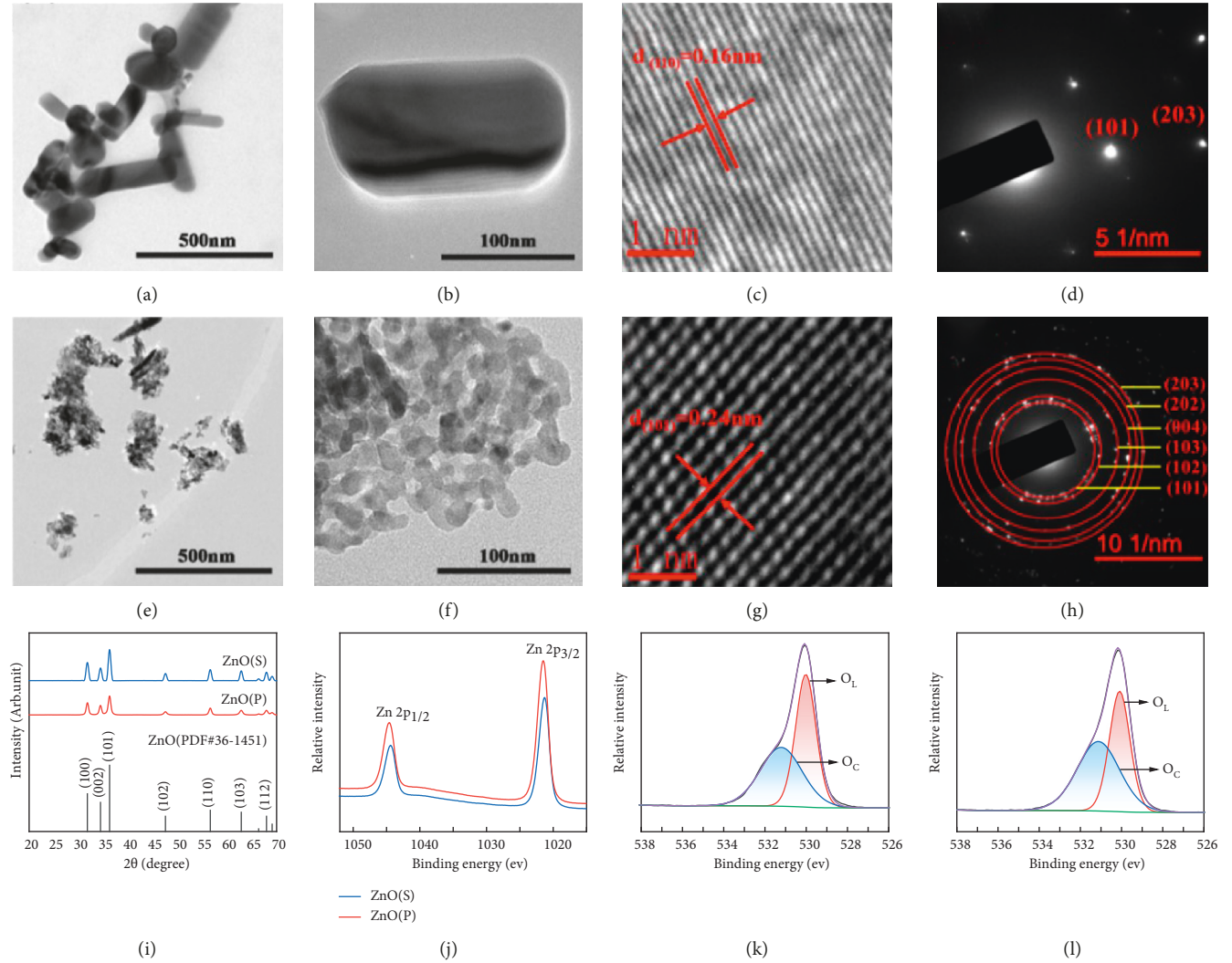


FIGURE 1: (a-b) TEM images of ZnO(S), (c) HRTEM images of ZnO(S), (d) SAED pattern of ZnO(S), (e-f) TEM images of ZnO(P), (g) HRTEM images of ZnO(P), (h) SAED pattern of ZnO(P), (i) WAXD patterns of ZnO(S) and ZnO(P), (j) XPS spectra of Zn 2p, (k) O 1s XPS spectra of ZnO(S), and (l) O 1s XPS spectra of ZnO(P).

temperature ( $\alpha_1$ ) is due to the melting of  $\alpha$ -crystal formed at  $T_c$ , while the higher temperature ( $\alpha_2$ ) is due to the melting of  $\alpha$ -crystal originated from  $\beta\alpha$ -recrystallization during heating [27], so the  $k_{\beta(DSC)}$  value should exclude the melting enthalpy of  $\alpha_2$ . The crystal melting areas of ZnO(S)/Pht/iPP and ZnO(P)/Pht/iPP are different, and ZnO(S)/Pht/iPP is mainly the melting of  $\alpha$ -crystal, while ZnO(P)/Pht/iPP is mainly the melting of  $\beta$ -crystal, and the  $k_{\beta(DSC)}$  value is calculated by equations (1) and (2); results are shown in Table 2. From Table 2, we can infer that the  $k_{\beta(DSC)}$  value of ZnO(S)/Pht/iPP is only 18.0%, whereas the  $k_{\beta(DSC)}$  value of ZnO(P)/Pht/iPP is up to 84.6%, demonstrating that the selectivity of  $\beta$ -crystal nucleation of ZnO(P)/Pht is better than that of ZnO(S)/Pht.

The impact strength and stress-strain behavior of nucleated iPP are strongly related to its content of  $\beta$ -crystal. Figure 2(c) presents the impact strength of pure iPP and nucleated iPP. Pure iPP behaved as a fragile and stiff material with weak impact strength. The addition of ZnO(S)/Pht and

ZnO(P)/Pht increased the toughness of iPP, and the impact strength of ZnO(S)/Pht/iPP and ZnO(P)/Pht/iPP is 1.4 times and 2.0 times greater than pure iPP, respectively. Figure 2(d) presents the stress-strain curves of pure iPP and nucleated iPP. It can be seen that pure iPP exhibited lower ductility; that is, the elongation at break (%) of pure iPP is only 127.7%. The addition of ZnO(S)/Pht and ZnO(P)/Pht reduced the stress and increased the strain of iPP. The elongation at break of ZnO(S)/Pht/iPP and ZnO(P)/Pht/iPP is 178.8% and 1219.9%, respectively. ZnO(P)/Pht/iPP has an excellent elongation at break, which is 9.6 times greater than pure iPP and is 6.8 times greater than ZnO(S)/Pht/iPP, respectively. The impact strength and stress-strain behavior further prove that the  $\beta$ -crystal nucleating efficiency of ZnO(P)/Pht is better than ZnO(S)/Pht.

POM can directly identify the  $\alpha$ -crystal and  $\beta$ -crystal of iPP due to their different optical properties, and the birefringence of  $\beta$ -crystal is much greater than  $\alpha$ -crystal resulting in  $\beta$ -crystal being brighter than  $\alpha$ -crystal [28].

TABLE 1: O 1s XPS spectra and BET surface area of ZnO samples.

Sample name	Relative percentage (%)		BET surface area ( $\text{m}^2\cdot\text{g}^{-1}$ )
	Lattice oxygen	Chemisorbed oxygen	
ZnO(S)	52.2	47.8	2.3
ZnO(P)	46.9	53.1	44.3

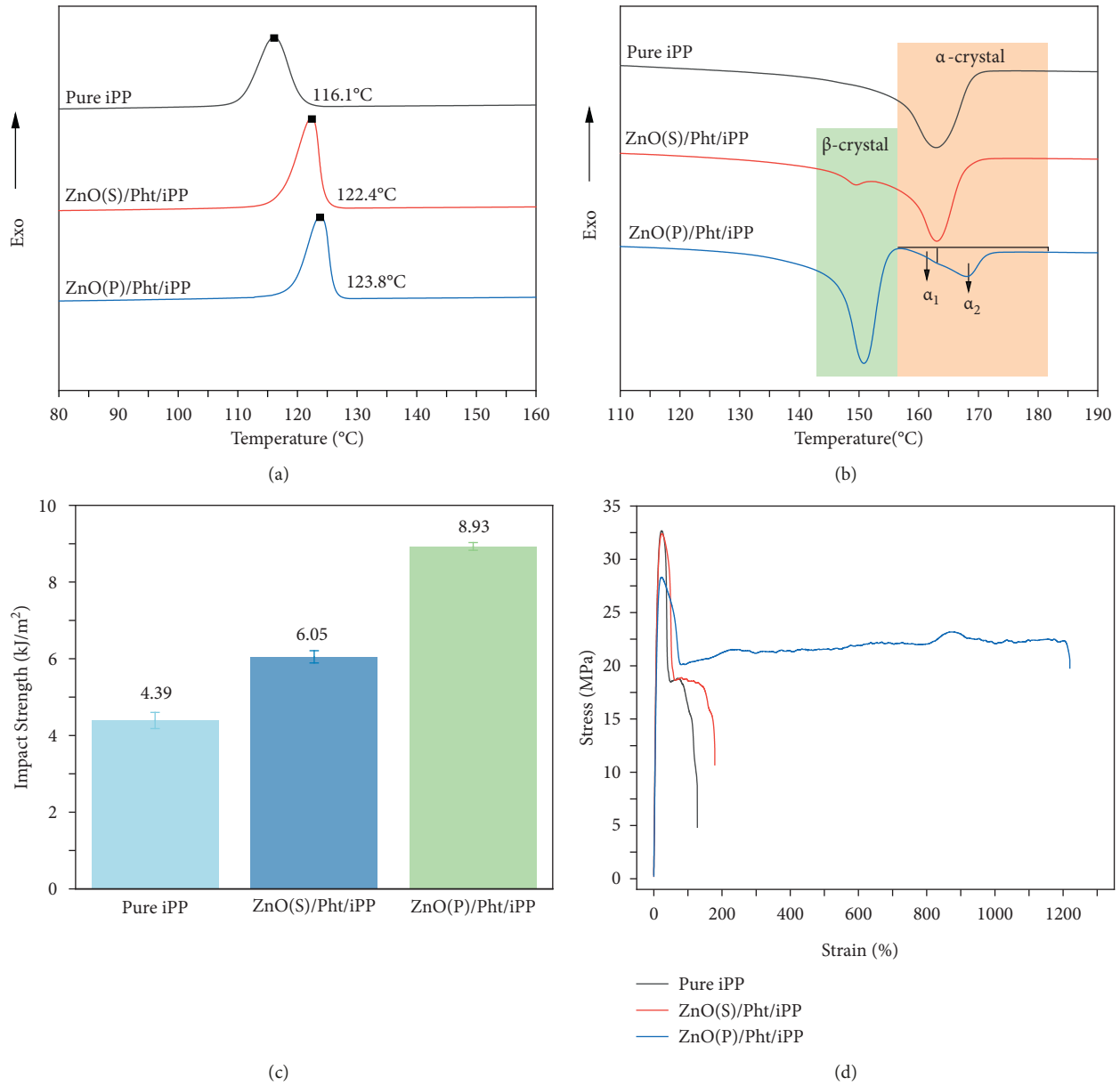


FIGURE 2: (a) DSC crystallization curves of pure iPP and nucleated iPP; (b) DSC melting curves of pure iPP and nucleated iPP; (c) impact strength of pure iPP and nucleated iPP; (d) stress-strain curves of pure iPP and nucleated iPP.

Therefore, it is another crucial and visual way when characterizing the  $\beta$ -crystal nucleation of nucleated iPP samples. Figure 3 presents the crystal morphologies of pure iPP and nucleated iPP. For pure iPP, only a few  $\alpha$ -crystals are presented after isothermal crystallization at  $130^\circ\text{C}$  for 10 min. With the addition of ZnO(S)/Pht and ZnO(P)/Pht, brighter  $\beta$ -crystals form in the iPP melt, in addition, the

number of crystals is more than that of pure iPP, and crystals are in contact with each other, indicating that the crystallization has been completed at 10 minutes. Although ZnO(S)/Pht and ZnO(P)/Pht can induce iPP to form  $\beta$ -crystals, the content of  $\beta$ -crystals of ZnO(P)/Pht/iPP is more than that of ZnO(S)/Pht/iPP, consistent with  $k_{\beta(\text{DSC})}$  values.

TABLE 2:  $\Delta H_{\alpha}$ ,  $\Delta H_{\beta}$ ,  $X_{\alpha}$ ,  $X_{\beta}$ , and  $k_{\beta(\text{DSC})}$  of pure iPP and nucleated iPP.

Sample name	$\Delta H_{\alpha 1}$ (J/g)	$\Delta H_{\alpha 2}$ (J/g)	$\Delta H_{\beta}$ (J/g)	$X_{\alpha 1}$ (%)	$X_{\alpha 2}$ (%)	$X_{\beta}$ (%)	$k_{\beta(\text{DSC})}$ (%)
Pure iPP	103.7	—	—	58.6	—	—	—
ZnO(S)/Pht/iPP	86.9	—	18.2	49.1	—	10.8	18.0
ZnO(P)/Pht/iPP	16.9	7.9	88.0	9.5	4.5	52.2	84.6

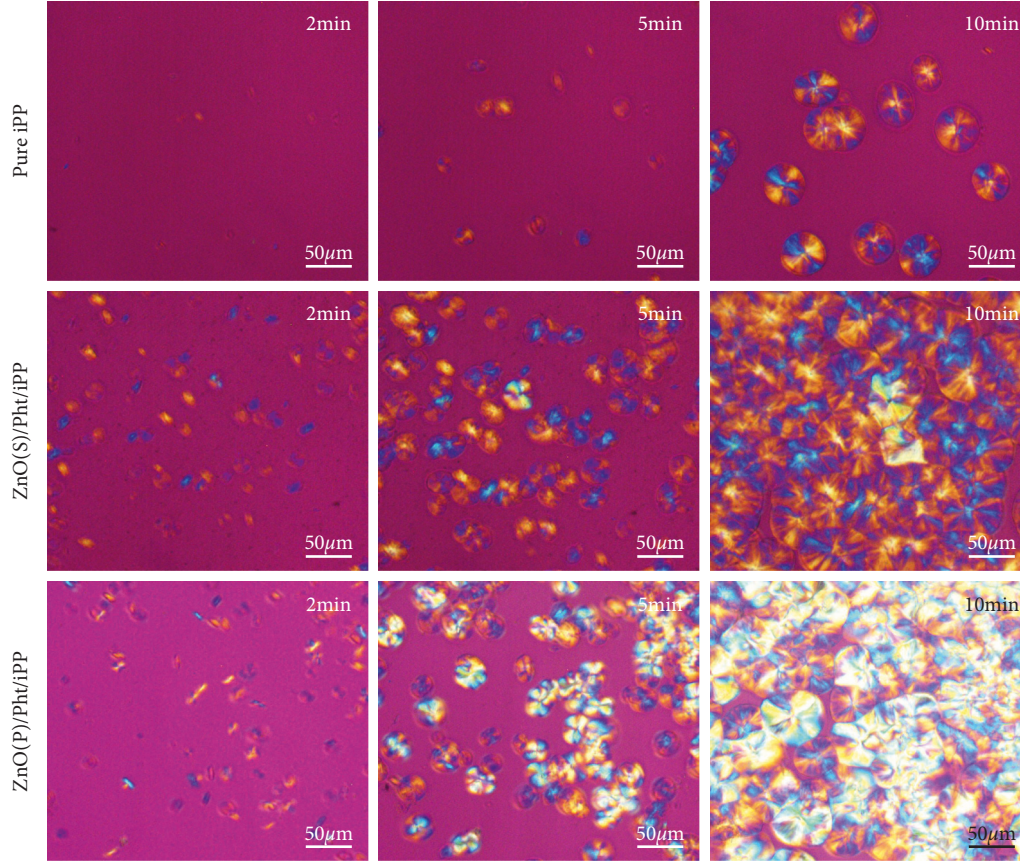


FIGURE 3: POM images of pure iPP and nucleated iPP crystallized at 130°C.

3.3. *Isothermal Crystallization Kinetics.* Isothermal crystallization kinetics is an available way to appraise nucleation efficiency. The relative crystallinity ( $X_t$ ) [29] of the composite can be calculated by the following equation:

$$X_t = \frac{\int_0^t (dH_c/dt)dt}{\int_0^{\infty} (dH_c/dt)dt}, \quad (3)$$

where  $dH_c/dt$  denotes the ratio of heat flow rate. Figure 4 displays the plots of  $X_t$  versus crystallization time ( $t$ ) for pure iPP and nucleated iPP. All curves present “S” shaped, indicating that the isothermal crystallization process is divided into three stages: it was no obvious change in  $X_t$  during crystallization induction; then  $X_t$  increases as  $t$  in the middle of crystallization; finally, these curves flatten out until  $X_t$  reaches its maximum. Interestingly, the  $t$  is shorter for ZnO(S) Pht/Ipp and ZnO(P) Pht/iPP compared with pure iPP at the same  $T_c$ . Thus, the incorporation of ZnO(S)/Pht and ZnO(P)/Pht into the iPP matrix has accelerated the isothermal crystallization process.

The Avrami equation [29–31] is also performed to further characterize isothermal crystallization, which is shown as follows:

$$1 - X_t = \exp(-kt^n), \quad (4)$$

where  $k$  is the crystallization rate constant and  $n$  is the Avrami exponent. The values of  $k$  and  $n$  can be calculated when (4) is transformed to the double logarithmic form as follows:

$$\ln[-\ln(1 - X_t)] = n \ln t + \ln k. \quad (5)$$

Plots of  $\ln[-\ln(1 - X_t)]$  versus  $\ln t$  are shown in Figure 5. From Figure 5, all curves show a good linear relationship, and the square of the correlation coefficient ( $R^2$ ) is above 0.99, indicating that the isothermal crystallization behavior of pure iPP and nucleated iPP can be described by the Avrami equation. The parameters  $k$  and  $n$  are the intersection and slope of the fitting curves, respectively, and the results are listed in Table 3. The crystallization half time

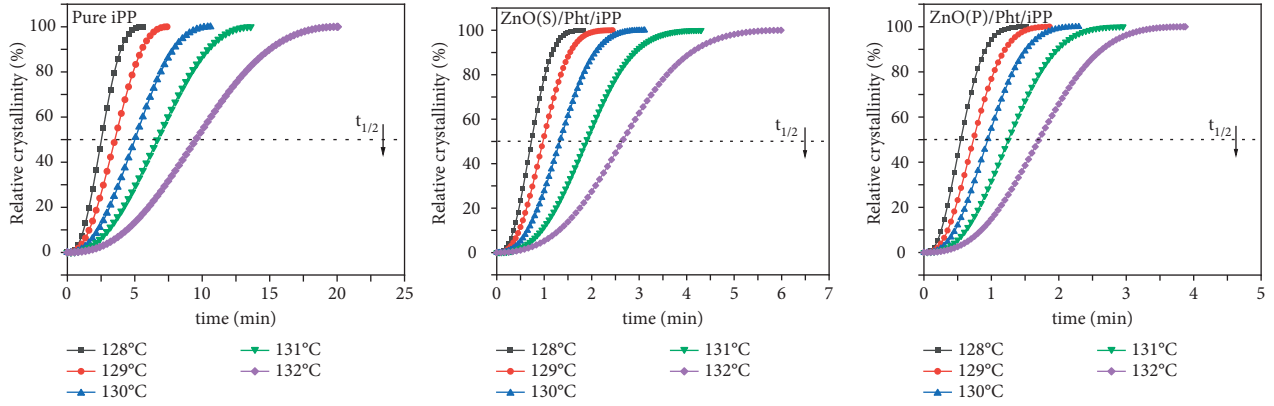
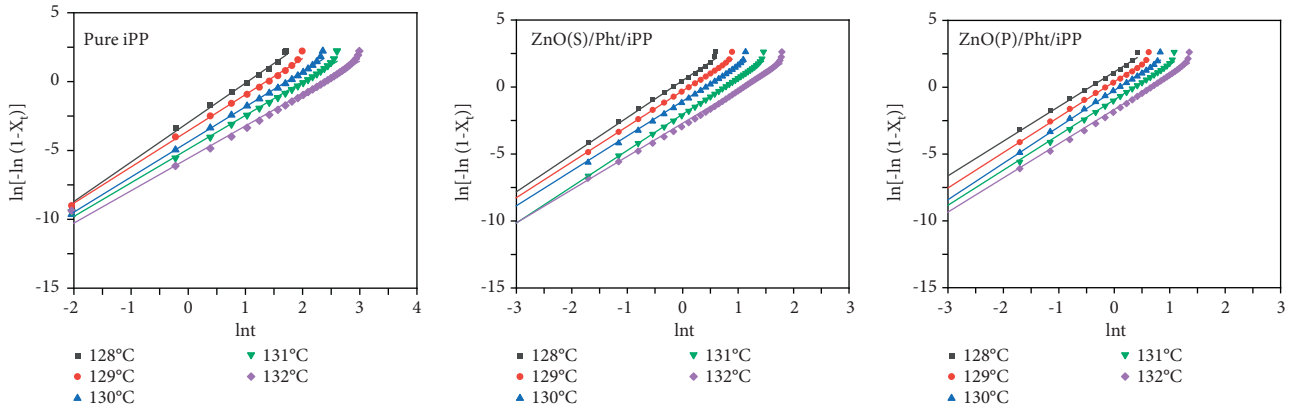


FIGURE 4: Plots of crystallinity versus crystallization time for pure iPP and nucleated iPP.


 FIGURE 5: Plots of  $\ln[-\ln(1-X_t)]$  versus  $lnt$  for pure iPP and nucleated iPP.

( $t_{1/2}$ ) can be calculated by the following equation (6) when we obtained the values of  $k$  and  $n$ :

$$t_{1/2} = \left( \frac{\ln 2}{k} \right)^{1/n} \quad (6)$$

The values of  $t_{1/2}$  are also summarized in Table 3.

From Table 3, the  $n$  values are found to vary slightly between 2.4 and 2.9 for both pure iPP and nucleated iPP. The almost unchanged  $n$  values indicate that the addition of ZnO(S)/Pht and ZnO(P)/Pht does not change the crystallization mechanism of iPP in the composites, relative to pure iPP. The  $n$  values are all close to 3, indicating that the crystallization mechanism may correspond to heterogeneous nucleation with three-dimensional crystal growth for pure iPP and nucleated iPP. In this work, the unit of  $k$  is  $\text{min}^{-n}$ , whereas  $n$  is not a constant; it is meaningless to use the  $k$  values for comparing the crystallization rate. The physical meaning of  $t_{1/2}$  is the time when achieving 50% of final crystallinity; therefore, a large value of  $t_{1/2}$  indicates a long crystallization time and a slow crystallization rate. For pure iPP and nucleated iPP, the  $t_{1/2}$  values increase with increasing  $T_c$ , indicating a slower crystallization rate at higher  $T_c$ . Meanwhile, compared with pure iPP, the  $t_{1/2}$  values decrease when adding ZnO(S)/Pht and ZnO(P)/Pht at the same  $T_c$ . For example, the  $t_{1/2}$  values of iPP decrease significantly from 4.8 min to 1.4 min and 1.1 min with the addition of ZnO(S)/

Pht and ZnO(P)/Pht when crystallized at 130°C, respectively. This indicates that the addition of ZnO(S)/Pht and ZnO(P)/Pht into iPP significantly enhances the crystallization rate of iPP; moreover, the crystallization rate of ZnO(P)/Pht/iPP is faster than that of ZnO(S)/Pht/iPP.

These results suggest that the nucleation efficiency of ZnO(P)/Pht is higher than that of ZnO(S)/Pht in iPP melt. The question of why the nucleation efficiency of ZnO(P)/Pht is higher than that of ZnO(S)/Pht has not previously been given a reasonable answer. According to the literature [1], we conclude that ZnO and Pht reacted to generate ZnPht during the process of extrusion at a temperature of 200°C. We consider that the difference in reaction of ZnO(S)/Pht and ZnO(P)/Pht may lead to the difference in  $\beta$ -crystal nucleation efficiencies of iPP. Therefore, ZnO(S) and ZnO(P) were mixed with Pht in a molar ratio of 1 : 1 and heated on a hot stage at 200°C for 5 min, named ZnO(S)/Pht-200°C and ZnO(P)/Pht-200°C, to simulate the process of extrusion. For comparison, ZnO(S)/Pht and ZnO(P)/Pht without any heat treatment named ZnO(S)/Pht-25°C and ZnO(P)/Pht-25°C were also prepared.

**3.4. Chemical Reaction of ZnO(S)/Pht and ZnO(P)/Pht.** FTIR spectrometer and WAXD investigation were used to discuss the structure evolution of the ZnO(S)/Pht and ZnO(P)/Pht. As shown in Figure 6(a), there is no characteristic peak for

TABLE 3: Isothermal crystallization parameters of pure iPP and nucleated iPP.

Sample name	$T_c$ (°C)	$n$	$k$ (min <sup>-n</sup> )	$t_{1/2}$ (min)	$R^2$
Pure iPP	128	2.9	0.05	2.5	0.994
	129	2.6	0.03	3.4	0.997
	130	2.6	0.01	4.8	0.996
	131	2.5	0.007	6.4	0.994
	132	2.4	0.004	9.2	0.992
ZnO(S)/Pht/iPP	128	2.8	0.9	0.9	0.998
	129	2.7	0.5	1.2	0.998
	130	2.6	0.3	1.4	0.994
	131	2.7	0.1	1.9	0.997
	132	2.5	0.05	2.4	0.992
ZnO(P)/Pht/iPP	128	2.6	2.0	0.6	0.998
	129	2.7	1.1	0.8	0.999
	130	2.7	0.6	1.1	0.999
	131	2.7	0.3	1.4	0.999
	132	2.8	0.1	1.9	0.999

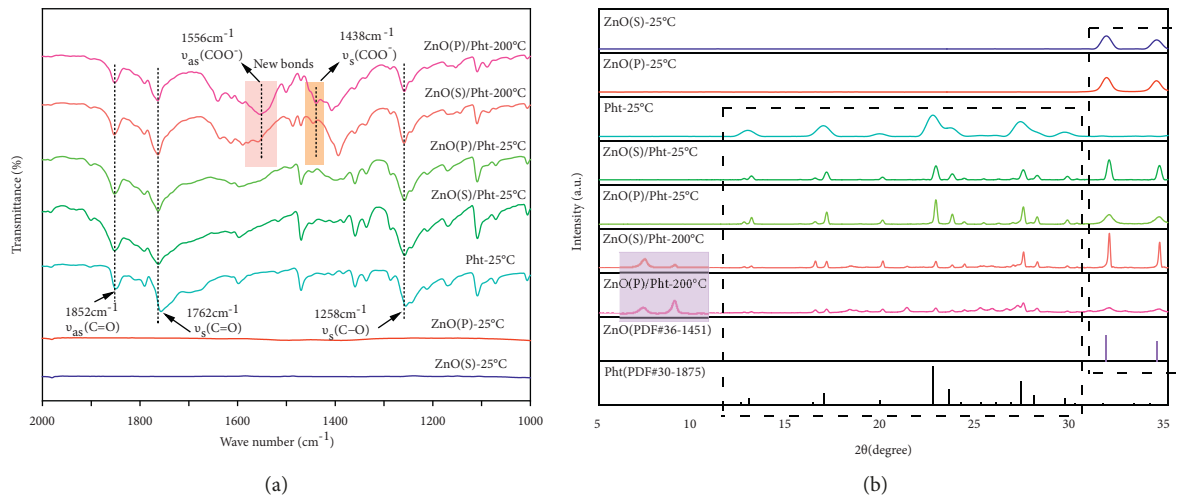
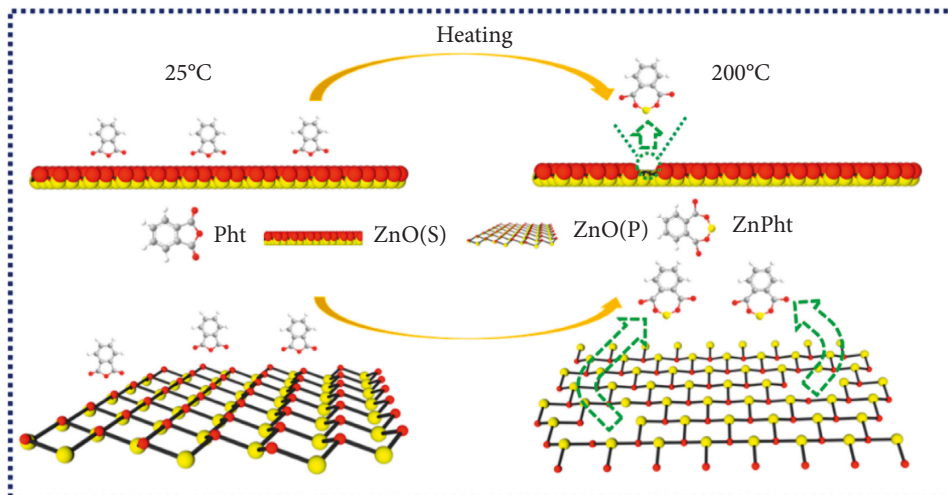


FIGURE 6: (a) FTIR spectra and (b) WAXD patterns.



SCHEME 1: Reaction mechanism of ZnO(S)/Pht and ZnO(P)/Pht.

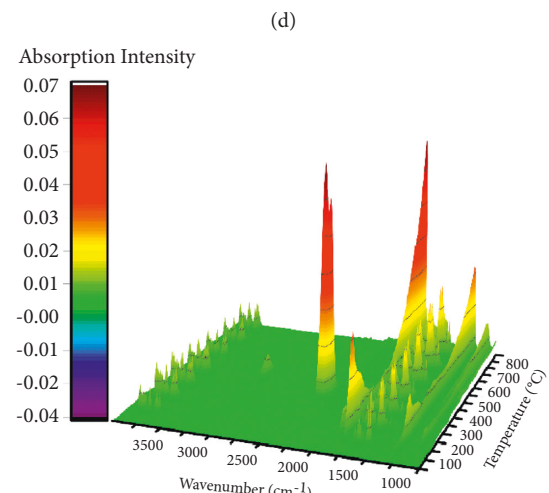
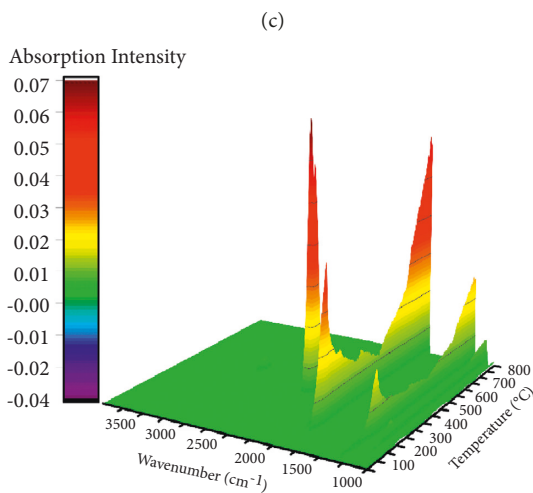
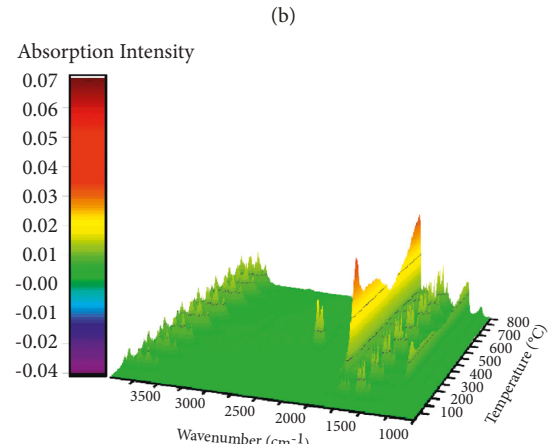
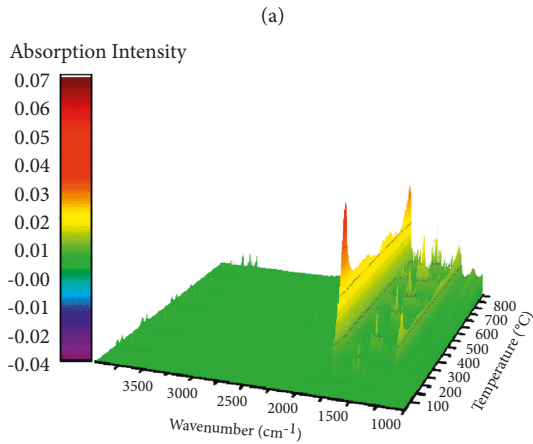
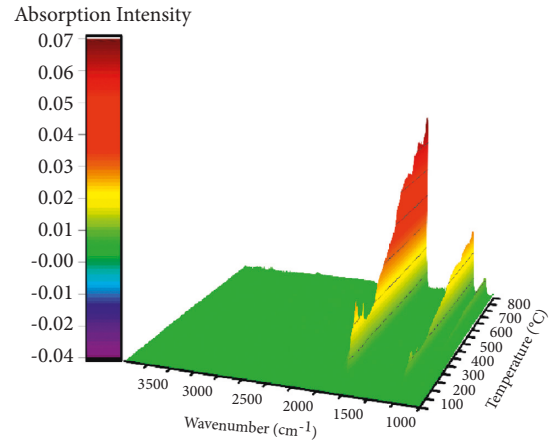
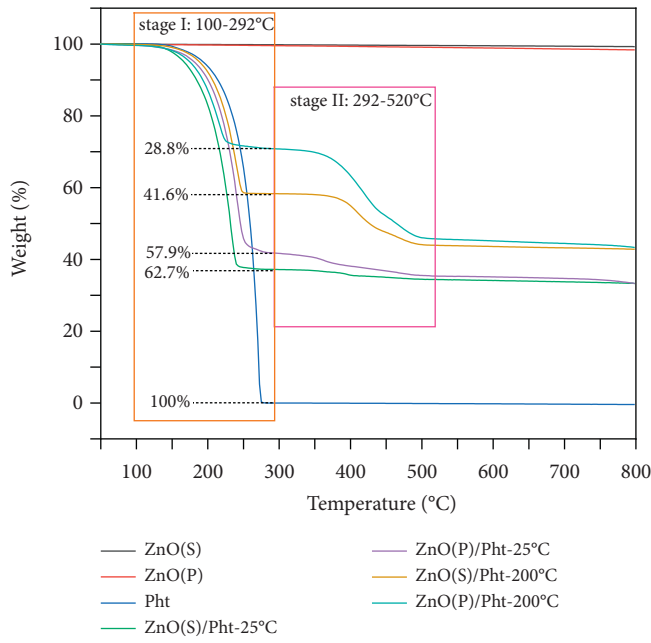


FIGURE 7: (a) TGA curves. (b) FTIR spectra of Pht. (c) FTIR spectra of ZnO(S)/Pht-25°C. (d) FTIR spectra of ZnO(P)/Pht-25°C. (e) FTIR spectra of ZnO(S)/Pht-200°C. (f) FTIR spectra of ZnO(P)/Pht-200°C.

ZnO(S) and ZnO(P) in the range  $2000\text{ cm}^{-1}$  to  $1000\text{ cm}^{-1}$ . Three characteristic peaks of Pht appeared at  $1852$ ,  $1762$ , and  $1258\text{ cm}^{-1}$ , corresponding to the antisymmetric stretching vibration of C=O units, symmetric stretching vibration of C=O units, and the stretching vibration of C-O units, respectively. For ZnO(S)/Pht-25°C and ZnO(P)/Pht-25°C, no new characteristic peaks appeared, indicating that no chemical reaction occurs at room temperature. However, for both ZnO(S)/Pht-200°C and ZnO(P)/Pht-200°C, except for the characteristic peaks Pht, two new absorption bands appear at  $1556$  and  $1438\text{ cm}^{-1}$ , corresponding to  $\text{COO}^-$  antisymmetric stretching vibration and  $\text{COO}^-$  symmetric stretching vibration, respectively. According to the literature [1], when the difference in wavenumber between  $\nu_{\text{as}}(\text{COO}^-)$  and  $\nu_{\text{s}}(\text{COO}^-)$  is low, ZnO reacts with Pht to generate ZnPht. The FTIR spectra of ZnO(S)/Pht-200°C and ZnO(P)/Pht-200°C featured almost the same characteristic peaks, indicating that parts of ZnO(S)/Pht and ZnO(P)/Pht reacted in 200°C to generate ZnPht.

From Figure 6(b), we can see the mixture of ZnO(S)/Pht-25°C and ZnO(P)/Pht-25°C only had the diffraction peaks of ZnO and Pht, and no new diffraction peaks appeared. However, for ZnO(S)/Pht-200°C and ZnO(P)/Pht-200°C, except for the diffraction peaks of ZnO and Pht, two new diffraction peaks appear at values of  $2\theta$  of approximately  $7.3^\circ$  and  $8.9^\circ$ , corresponding to the diffraction peaks of ZnPht. Thus, the result of WAXD further refers that parts of ZnO(S)/Pht and ZnO(P)/Pht reacted at 200°C to form ZnPht.

**3.5. Mechanism of Nucleation Difference between ZnO(S)/Pht and ZnO(P)/Pht.** Although both ZnO(S) and ZnO(P) react with Pht to generate ZnPht, we considered that ZnO(P) reacts with Pht easier than ZnO(S), and the contents of react product, that is, ZnPht, are higher, leading to a high content of  $\beta$ -crystal. The mechanism is illustrated in Scheme 1. Firstly, during the heating process, Pht melts, and being ZnO(P) with a large number of crystal grains and small crystal grains size, the probability of reaction with Pht is greater. Secondly, ZnO(P) has a large BET surface area than ZnO(S), resulting in a more adequate reaction with Pht. The most important point is that ZnO(P) has higher reactivity than ZnO(S) because of its more chemisorbed oxygen or OH; under the same conditions, it is easier to react with Pht. Therefore, ZnO(P) reacts with Pht to generate more ZnPht.

Due to the difference in the thermal stability of ZnO, Pht, and ZnPht, thermogravimetric infrared spectroscopy analysis was performed to prove the proposed mechanism. As shown in Figure 7, from the TGA curves, it can be seen that ZnO(S) and ZnO(P) almost have no thermal decomposition because of their excellent thermal stability. Pht shows one distinct weight-loss stage: the one is at  $130\text{--}292^\circ\text{C}$  with 100% mass loss, which is attributed to the sublimation of Pht. However, the decomposition process of ZnO(S)/Pht-25°C, ZnO(P)/Pht-25°C, ZnO(S)/Pht-200°C, and ZnO(P)/Pht-200°C shows two weight-loss stages: the first one is at  $130\text{--}292^\circ\text{C}$  and the second one is at  $305\text{--}518^\circ\text{C}$ . From the infrared spectra of Pht-25°C, ZnO(S)/Pht-25°C, ZnO(P)/Pht-25°C, ZnO(S)/Pht-200°C, and ZnO(P)/Pht-200°C, we

can see clearly that three peaks appeared at  $1852\text{ cm}^{-1}$ ,  $1762\text{ cm}^{-1}$ , and  $1258\text{ cm}^{-1}$  when the temperature up to  $130^\circ\text{C}$  is applied, corresponding to characteristic peaks of Pht. One peak appeared at  $2358\text{ cm}^{-1}$  when a temperature of  $305^\circ\text{C}$  is applied, which is attributed to the characteristic peaks of  $\text{CO}_2$  produced by the thermal decomposition of ZnPht [32]. Therefore, the first stage and the second stage are attributed to the thermal decomposition of Pht and ZnPht, respectively. For ZnO(S)/Pht-25°C, ZnO(P)/Pht-25°C, ZnO(S)/Pht-200°C, and ZnO(P)/Pht-200°C, part of Pht sublimates and the other part generate ZnPht; thereby, we can calculate the mass of ZnPht by the following equations:

$$m = \frac{M_1}{M}, \quad (7)$$

where  $m$  represents the mass of Pht in the mixture,  $M$  represents the total molar mass of the mixture, and  $M_1$  represents the molar mass of Pht. Therefore, the mass of ZnPht can be calculated by

$$m_2 = \frac{m - m_1}{m}, \quad (8)$$

where  $m_2$  represents the mass of ZnPht, and  $m_1$  represents the mass loss in first stage for ZnO(S)/Pht-25°C, ZnO(P)/Pht-25°C, ZnO(S)/Pht-200°C, and ZnO(P)/Pht-200°C. Therefore, the mass of ZnPht in ZnO(S)/Pht-25°C, ZnO(P)/Pht-25°C, ZnO(S)/Pht-200°C, and ZnO(P)/Pht-200°C is 2.8%, 10.2%, 35.5%, and 55.3%, respectively. Therefore, ZnO(S)/Pht-25°C and ZnO(P)/Pht-25°C, or ZnO(S)/Pht-200°C and ZnO(P)/Pht-200°C and ZnO(P) react with Pht to generate more ZnPht than ZnO(S) under same conditions.

## 4. Conclusions

In this work, ZnO(S) and ZnO(P) have been chosen to induce  $\beta$ -iPP in situ with the presence of Pht. The crystallization and melting behaviors, the values of  $k_{\beta(\text{DSC})}$ , impact strength and strain-stress curves, and isothermal crystallization kinetics were well investigated. The unique crystalline characteristic effect of in situ interaction between ZnO and Pht on inducing  $\beta$  nucleation of iPP was found. Compared to ZnO(S)/Pht, ZnO(P)/Pht has the selectivity of  $\beta$ -crystal nucleation during the crystallization of iPP. We propose a new mechanism that the content of ZnPht generated by ZnO(P)/Pht is more than that of ZnO(S)/Pht during its in situ reaction. FTIR spectroscopy, WAXD, and TG-IR analysis were consistent with this mechanism. This work may provide a new perspective to control the crystal type of polymorphic polymer by adjusting the crystalline characteristic of the nucleating agent.

## Data Availability

The data used to support the findings of this study are included within the article.

## Conflicts of Interest

The authors declare that they have no conflicts of interest.

## Acknowledgments

The authors gratefully acknowledge the financial support from the National Key R&D Program of China (2018YFC1903500), Science and Technology Project of Guizhou Province ((2019)2867 and (2019)5640), and Graduate Research Fund of Guizhou Province (YJSCXJH[2020]032).

## References

- [1] W. Qin, Z. Xin, C. M. Pan, S. Sun, X. Jiang, and S. Zhao, "In situ formation of zinc phthalate as a highly dispersed  $\beta$ -nucleating agent for mechanically strengthened isotactic polypropylene," *Chemical Engineering Journal*, vol. 358, pp. 1243–1252, 2019.
- [2] Y. C. Shen, H. C. Tian, W. L. Pan et al., "Unexpected improvement of both mechanical strength and elasticity of EPDM/PP thermoplastic vulcanizates by introducing  $\beta$ -nucleating agents," *Macromolecules*, vol. 54, no. 6, pp. 2835–2843, 2021.
- [3] S. Z. Zhao, W. Qin, Z. Xin et al., "In situ generation of a self-dispersed  $\beta$ -nucleating agent with increased nucleation efficiency in isotactic polypropylene," *Polymer*, vol. 151, pp. 84–91, 2018.
- [4] B. J. Luo, H. F. Li, Y. Zhang et al., "Wall slip effect on shear-induced crystallization behavior of isotactic polypropylene containing  $\beta$ -nucleating agent," *Industrial & Engineering Chemistry Research*, vol. 53, no. 34, pp. 13513–13521, 2014.
- [5] Z. Zhang, C. Wang, Z. Yang, C. Chen, and K. Mai, "Crystallization behavior and melting characteristics of PP nucleated by a novel supported  $\beta$ -nucleating agent," *Polymer*, vol. 49, no. 23, pp. 5137–5145, 2008.
- [6] J. Varga and J. Karger-Kocsis, "Interfacial morphologies in carbon fibre-reinforced polypropylene microcomposites," *Polymer*, vol. 36, no. 25, pp. 4877–4881, 1995.
- [7] J. Varga, " $\beta$ -modification of isotactic polypropylene: preparation, structure, processing, properties, and application," *Journal of Macromolecular Science Part B*, vol. 41, no. 4-6, pp. 1121–1171, 2002.
- [8] Y. F. Zhang, D. Li, and Q. J. Chen, "Preparation and nucleation effects of nucleating agent hexahydrophthalic acid metal salts for isotactic polypropylene," *Colloid & Polymer Science*, vol. 295, no. 10, pp. 1973–1982, 2017.
- [9] C. Y. Zhang, B. Wang, J. J. Yang et al., "Synergies among the self-assembled  $\beta$ -nucleating agent and the sheared isotactic polypropylene matrix," *Polymer*, vol. 60, pp. 40–49, 2015.
- [10] A. J. Lovinger, J. O. Chua, and C. C. Gryte, "Studies on the  $\alpha$  and  $\beta$  forms of isotactic polypropylene by crystallization in a temperature gradient," *Journal of Polymer Science Polymer Physics Edition*, vol. 15, no. 4, pp. 641–656, 1977.
- [11] H. Dragaun, H. Hubeny, and H. Muschik, "Shear-induced  $\beta$ -form crystallization in isotactic polypropylene," *Journal of Polymer Science Polymer Physics Edition*, vol. 15, no. 10, pp. 1779–1789, 1977.
- [12] S. Z. Zhao, K. H. Liu, S. Zhou, Y. Shi, and Z. Xin, "A novel self-dispersed  $\beta$  nucleating agent for isotactic polypropylene and its unique nucleation behavior and mechanism," *Polymer*, vol. 132, pp. 69–78, 2017.
- [13] S. Zhao, H. Gong, X. Yu et al., "A highly active and selective  $\beta$ -nucleating agent for isotactic polypropylene and crystallization behavior of  $\beta$ -nucleated isotactic polypropylene under rapid cooling," *Journal of Applied Polymer Science*, vol. 133, no. 32, Article ID 43767, 2016.
- [14] W. Qin, K. H. Liu, Z. Xin, H. Ling, S. Zhou, and S. Zhao, "Zinc pimelate as an effective  $\beta$ -nucleating agent for isotactic polypropylene at elevated pressures and under rapid cooling rates," *Polymer Crystallization*, vol. 3, no. 3, 2020.
- [15] Z. He, Y. F. Zhang, and Y. Li, "Dependence of  $\beta$ -crystal formation of isotactic polypropylene on crystallization conditions," *Journal of Polymer Research*, vol. 27, no. 9, p. 250, 2020.
- [16] L. Y. Liu, Y. Zhao, C. B. Zhang, Z. Dong, K. Wang, and D. Wang, "Morphological characteristics of  $\beta$ -Nucleating agents governing the formation of the crystalline structure of isotactic Polypropylene," *Macromolecules*, vol. 54, no. 14, pp. 6824–6834, 2021.
- [17] Q. L. Lu and Q. Dou, " $\beta$ -Crystal formation of isotactic polypropylene induced by N, N'-dicyclohexylsuccinamide," *Journal of Polymer Research*, vol. 16, no. 5, pp. 555–560, 2009.
- [18] M. Dong, Z. X. Guo, J. Yu, and Z. Su, "Crystallization behavior and morphological development of isotactic polypropylene with an aryl amide derivative as  $\beta$ -form nucleating agent," *Journal of Polymer Science Part B: Polymer Physics*, vol. 46, no. 16, pp. 1725–1733, 2008.
- [19] Y. Yue, X. X. Wang, and J. C. Feng, "Concentration effect of a bis-amide nucleating agent on the shear-induced crystallization behavior of isotactic polypropylene," *ACS Applied Polymer Materials*, vol. 3, no. 2, pp. 1145–1156, 2021.
- [20] G. Y. Shi, X. D. Zhang, Y. H. Cao, and J. Hong, "Melting behavior and crystalline order of  $\beta$ -crystalline phase polypropylene," *Makromolekulare Chemie*, vol. 194, no. 1, pp. 269–277, 1993.
- [21] Q. Dou, Q. L. Lu, and H. D. Li, "Effect of metallic salts of malonic acid on the formation of  $\beta$  crystalline form in isotactic polypropylene," *Journal of Macromolecular Science, Part B*, vol. 47, no. 5, pp. 900–912, 2008.
- [22] J. X. Li, W. L. Cheung, and D. Jia, "A study on the heat of fusion of beta-polypropylene," *Polymer*, vol. 40, no. 5, pp. 1219–1222, 1999.
- [23] L. Jing, Z. Xu, X. Sun, J. Shang, and W. Cai, "The surface properties and Photocatalytic activities of ZnO ultrafine particles," *Applied Surface Science*, vol. 180, no. 3-4, pp. 308–314, 2001.
- [24] K. M. Lin, Y. Y. Chen, and C. Y. Chiu, "Effects of growth behaviors on chemical and physical properties of sol-gel derived ZnO: Ga films," *Journal of Sol-Gel Science and Technology*, vol. 55, no. 3, pp. 299–305, 2010.
- [25] A. H. Boonstra and C. A. H. A. Mutsaers, "Relation between the photoabsorption of Oxygen and the number of hydroxyl groups on a Titanium dioxide surface," *Journal of Physical Chemistry*, vol. 79, pp. 1694–1698, 1974.
- [26] Y. Wang, R. Shi, J. Lin, and Y. Zhu, "Enhancement of photocurrent and photocatalytic activity of ZnO hybridized with graphite-like C<sub>3</sub>N<sub>4</sub>," *Energy & Environmental Science*, vol. 4, no. 8, pp. 2922–2929, 2011.
- [27] J. Varga, "Melting memory effect of the  $\beta$ -modification of polypropylene," *Journal of Thermal Analysis*, vol. 31, no. 1, pp. 165–172, 1986.
- [28] B. Lotz, " $\alpha$  and  $\beta$  phases of isotactic polypropylene: a case of growth kinetics 'phase reentrancy' in polymer crystallization," *Polymer*, vol. 39, no. 19, pp. 4561–4567, 1998.
- [29] G. Z. Papageorgiou, D. S. Achilias, D. N. Bikiaris, and G. P. Karayannidis, "Crystallization kinetics and nucleation activity of filler in polypropylene/surface-treated SiO<sub>2</sub> nanocomposites," *Thermochimica Acta*, vol. 427, no. 1-2, pp. 117–128, 2005.

- [30] X. J. Jing and Z. B. Qiu, "Effect of low thermally reduced graphene loadings on the crystallization kinetics and morphology of biodegradable Poly (3-hydroxybutyrate)," *Industrial & Engineering Chemistry Research*, vol. 51, no. 42, pp. 13686–13691, 2012.
- [31] Z. B. Qiu and Z. S. Li, "Effect of orotic acid on the crystallization kinetics and morphology of biodegradable Poly (L-lactide) as an efficient nucleating agent," *Industrial & Engineering Chemistry Research*, vol. 50, no. 21, pp. 12299–12303, 2011.
- [32] J. T. Sun, D. L. Wang, K. L. Zhang, and W. Chunlin, "Synthesis, infrared spectra and crystal structures of zinc phthalate complexes," *Chinese Journal of Applied Chemistry*, vol. 14, pp. 99-100, 1997.